ISSN 2354-9114 (online), ISSN 0024-9521 (print)
Indonesian Journal of Geography Vol 57, No.2 (2025): 342 - 356
DOI: 10.22146/ijg.96391 website: https://jurnal.ugm.ac.id/ijg
©2025 Faculty of Geography UGM and The Indonesian Geographers Association

INDONESIAN JOURNAL OF GEOGRAPHY

RESEARCH ARTICLE

Measuring the Height of Volcanic Clouds Using Weather Radar: A Case Study of Mount Sinabung Eruptions in Medan, Indonesia

Hesti Heningtiyas[1], Budhi Achmadi[1], Asep Adang Supriyadi[1], Syachrul Arief[3], Rindita Charolydya[4]

[1] Sensing Technology Study Program, Faculty of Defense Science and Technology, Republic of Indonesia Defense University IPSC, Sentul Area, Citereup, Bogor, West Java, Indonesia
[2] Commander of the National Air Operations Command which covers central Indonesia
[3] Geospatial Information Agency, BIG, Bogor, 16911, Indonesia
[4] Meteorological, Climatological, and Geophysics Agency, BMKG, Jakarta, Indonesia

Received: 2024-05-24
Revised: 2025-06-26
Accepted: 2025-08-15
Published: 2025-08-19

Keywords: weather radar, HYSPLIT model, remote sensing, height of volcanic

Correspondent email: hesti.heningtiyas@tp.idu.ac.id, hesti.heningtiyas@bmkg.go.id

Abstract Weather radar is often used to observe volcanic eruptions and hydrometeorological phenomena. The reflectivity data of radar can describe the estimated height of volcanic eruptions while the Hybrid Single-Particle Lagrangian Integrated Trajectory (HYSPLIT) model explains the trajectory or direction of distribution of eruption clouds. The single polarization C-Band weather radar of BMKG at the Regional Office I in Medan was able to observe several eruptions of Mount Sinabung located at approximately 50 km which was considered to be within the coverage area. Several eruptive activities were observed using Maximum (MAX) and VCUT (Vertical Cut) products to obtain information related to the height and characteristics. Meanwhile, the HYSPLIT model developed by ARL-NOAA was used to determine the direction of distribution of volcanic ash immediately after the eruption. The MAX and VCUT weather radar products as well as the NOAA HYSPLIT model applied to several events showed that the eruption height observed through weather radar was higher than the HYSPLIT model. Moreover, the direction of volcanic ash distribution was different from Volcanic Observatory Notice for Aviation (VONA) observations.

©2025 by the authors and Indonesian Journal of Geography
This article is an open access article distributed under the terms and conditions of the Creative Commons Attribution(CC BY NC) licensehttps://creativecommons.org/licenses/by-nc/4.0/.

1. Introduction

Indonesia is a country with the largest series of active volcanoes in the world because it passes through The Ring of Fire (Ariyanti et al., 2020; Nasruddin et al., 2016). The Ministry of Energy and Mineral Resources (ESDM) reported 69 volcanoes under the 24-hour monitoring or supervision of the Center for Volcanology and Geological Disaster Mitigation (PVMBG) out of a total of 127 active volcanoes in Indonesia. The observation spanned 7,000 km which spread across Sumatra, Java, Bali, Nusa Tenggara, Banda, Halmahera, to northern Sulawesi as presented in Figure 1.

Explosive volcanic eruptions are capable of ejecting large amounts of particles, aerosols and gases into the atmosphere, travel several thousand kilometers, and remain in the air for many days or months (Rizza et al., 2021). There are numerous direct and indirect dangers and impacts (Hapsari et al., 2020). Some of these can be in the form of volcanic ash (Webley & Mastin, 2009) and lava appearing on the surface with the exhalations of volcanic material caused by seismic energy, gas emissions such as sulfur dioxide SO2 (Marshall et al., 2022), and ground surface deformation (Poland et al., 2020). Moreover, volcanic eruptions have a disastrous impact on both the social and economic aspects of human lives (Aliotta et al., 2023; Marzano, Vulpiani, et al., 2006; Paredes-Mariño et al., 2022). The short-term impact can disrupt aviation activities (Prata, 2020) and safety (Marzano, Barbieri, et al., 2006) through flight delays and airport closures (Reichardt et al., 2019) to cause economic losses (Hirtl et al., 2020) and even more fatal consequences in the form of mid-air accidents. For example, British Airways plane experienced engine problems at a cruising altitude of 37,000 feet and had to make an emergency landing at Halim Perdana Kusuma Airport due to the eruption of Mount Galunggung in 1982 (Durant et al., 2010; Takebayashi et al., 2021).

Volcanic eruptions cause public health problems (Durant et al., 2010) around the location and surrounding areas (Carlsen et al., 2019). The long-term impact is in the form of climate change on Earth (Marshall et al., 2022; Marzano, Picciotti, et al., 2013; Rizza et al., 2021). An example was the eruption of Mount Toba tens of thousands of years ago which led to an extreme decrease in global temperatures during volcanic winter (Black et al., 2021; Osipov et al., 2020). These short- and long-term impacts show the need to understand the characteristics of eruptions with the aim of designing mitigation strategies.

Cloud height and volcanic ash distribution can be observed directly or based on radar or satellite analysis (Cahalan et al., 2023). This is necessary because the Flight Level (FL) information from Volcanic Ash Advisory Center (VAAC) is often used to provide Volcanic Ash Advisory (VAA) (Crawford et al., 2022) for flight safety (Engwell et al., 2021). The process requires submitting the direct eruption

Figure 1. Number and types of active volcanoes in Indonesia (Source:magma.esdm.go.id, 2021)

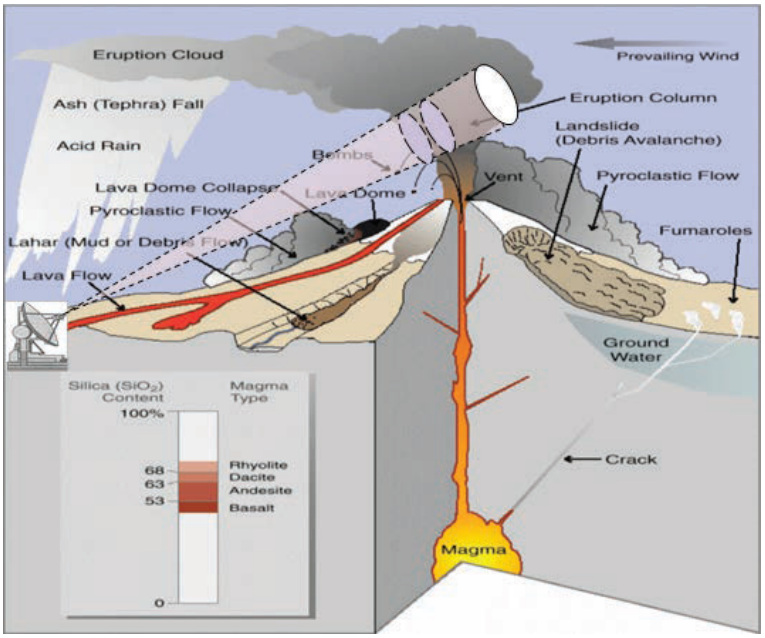

Figure 2. Schematic of volcano observations made by weather radar (Marzano, Picciotti, et al., 2013)

observations to VAAC in the form of Volcanic Observatory Notice for Aviation (VONA) report which includes information on the time of the eruption, volcanic activity, intensity, and height of the observed eruption clouds (Engwell et al., 2021). In Indonesia, the monitoring of eruptions and formation of VONA is through the PVMBG under the Ministry of Energy and Mineral Resources. However, the direct visual observation to determine the height of the eruption is often conducted subjectively without using specific tools and this leads to some limitations for the data.

Weather radar is designed to be used in observing hydrometeorological phenomena as well as volcanic eruptions (Marzano et al., 2011). The application of the tool for volcanic eruptions is presented in Figure 2. Some limitations are often identified which include estimation errors due to the influence of beam width (Sato, 2021) and refraction in the atmosphere but the tool is effective in monitoring volcanic eruptions specifically in cloudy conditions (Sato et al., 2018).

The characteristics of eruption ash is another parameter that can be determined using weather radar in addition to the

observe of the height of volcanic eruption clouds. For example, tephra is a type of volcanic material exhaled along with the clouds and gases formed during eruptions and is often termed a plume or ash cloud (Falconi & Marzano, 2019; Maki, Kim, et al., 2021). This material is capable of causing harm to the communities around the volcano (Poulidis et al., 2021). Moreover, tephra is divided into several types as presented in Table 1 (Maki, Kim, et al., 2021; Marzano, Picciotti, et al., 2013).

The information produced by weather radar includes doppler reflectivity and radial velocity data (Sokol et al., 2021). The reflectivity data can estimate the height of volcanic eruptions based on vertical profile reconstruction (Maki, Kim, et al., 2021; Marzano et al., 2011; Marzano, Lamantea, et al., 2013) while tephra size data is used to approximate the mass distribution of the entire plume (Maki, Kim, et al., 2021; Maki, Takaoka, et al., 2021). This study aims to measure the height of eruption clouds during volcanic eruption using weather radar and compare the results with the direct observations recorded through VONA information.

Several previous studies have used weather radar data to identify volcanic ash by estimating the concentration and rate of ash fall (Irwandi et al., 2019; Marzano et al., 2007, 2010). However, the information on the height of the eruption has not been widely examined. Eruption height information can affect the output of the Hybrid Single-Particle Lagrangian Integrated Trajectory (HYSPLIT) and other models. This study describes the differences in eruption height input and the results of models developed for information on the trajectory and dispersion of volcanic ash. The importance is associated with the fact that volcanic ash is dangerous for both public and aviation safety (Marzano, 2011). Therefore, the application of weather radar to mitigate the impact of volcanic ash distribution is useful for aviation safety and also beneficial for the public interest.

MOUNT SINABUNG

Mount Sinabung is a volcano that has become active again after a "long sleep" as observed from the absence of explosive eruptive activity before August-September 2010 (Global Volcanism Program, 2022; Nakada et al., 2019). The area is located in the Karo Regency of North Sumatra at coordinates 3˚10' N and 98˚23.5' E with a height of 2460 m above sea level (https://web.karokab.go.id).

MEDAN WEATHER RADAR CHARACTERISTICS

The Medan regional office has a C-Band Single Polarization Doppler weather radar which is operated by BMKG at the Center for Meteorology, Climatology and Geophysics Region I, Medan City, North Sumatra. The coordinates are at 3˚32' N and 98˚38' E which is approximately 50 km away northeast of Mount Sinabung as shown in Figure 3.

A weather radar can capture the peak of volcanic eruption when the scanning strategy covers the height of the mountain (Cahalan et al., 2023). Figure 4 shows the scanning strategy of the Medan weather radar at different elevation angles relative

Table 1. Classification of Eruption Ash Types (adapted from Marzano, et.al 2013 and Gematronic Weather Radar Systems Software Manual)

Tephra	Particle type	Typical particle size	Radar Classification	Distance from the volcano vent	Residence time in atmosphere
Ash	FA	<64 μm	-12 to -13 dBz	Hundreds to thousands of km	Days to months or years
	CA	64 - 532 μm	16 - 17 dBz	Tens to hundreds of km	Days
Lapili	SL	0.532 - 2.56 mm	46 - 47 dBz	Few to tens of km	Few minutes
	LL	2.56 - 32 mm	63 - 64 dBz	Hundreds of meters to a few of km	Seconds to minutes
Blocks	BB	> 32 mm	not detected	Tens to hundreds of m	Tens of seconds

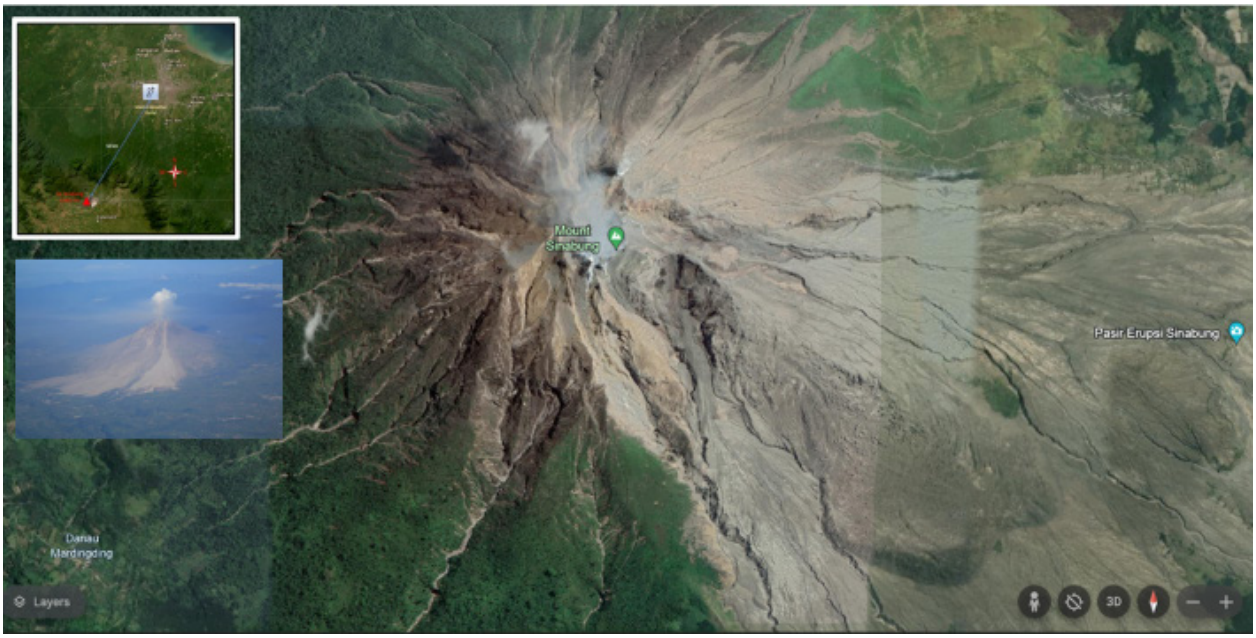

Figure 3. Location and Position of the Medan Weather Radar towards Mount Sinabung Mapped from Google Earth Pro

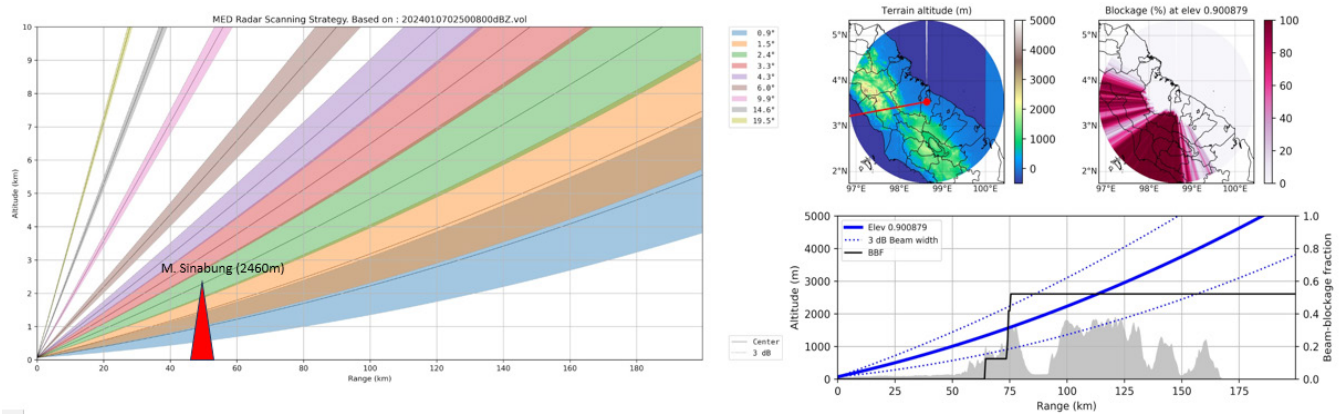

Figure 4. Scanning Strategy of the Medan Weather Radar (Source: SIDARMA BMKG)

Table 2. Comparison of Observation Results on the Height of Mount Sinabung Eruption

Date	West Indonesia Time (WIB)	UTC	Volcanic Ash Movement	Estimated Height of Eruption Cloud (m) VONA	Estimated Height of Eruption Cloud (m) Medan Weather Radar
28-Jul-21		06.10			6900
	13.20	06.20	E-S	4500	6900
		06.30			7300
		06.40			7900
07-May-21	09.08	02.08	E	2800	4570
	15.19	08.19	NE-E	3000	4600
		08.30			4400
		08.40			4430
		08.50			4470
		09.00			6430
		09.10			6470
		09.20			6530
		09.30			6700
		09.40			6400
		09.50			7430
		10.00			10000
		10.10			4700
19-Aug-20	18.23	11.23	E-SE	4000	NA
		11.30			7000
		11.40			7130
14-Aug-20		03.20			7200
	10.30	03.30	SE-S	2100	7000
		03.40			4800
	16.56	09.56	E	4200	7000
		10.10			6700
		10.20			3400
10-Aug-20	10.16	03.16	E-SE	5000	7000
		03.40	E-SE		2600

Source: ESDM, 2024 and the results of Medan Weather Radar data processing

to the Volume Coverage Pattern (VCP) 21 scanning mode. It is observed to have the capacity to capture the phenomenon of the eruption of Mount Sinabung effectively.

2. Methodology

DATA AND METHODS

The method used in this study was the descriptive analysis with a focus on the Medan weather radar observation data to identify the characteristics of clutter in the environment covered as presented in Figure 5. Clutter identification was implemented to minimize errors in identifying low-intensity volcanic ash which generally resembled the clutter. This was followed by the application of the quality control (QC) or clutter filtering process using the 3DCDP algorithm feature available in the Rainbow application version 5.49. Subsequently, the raw radar observation data were processed based on information related to the eruption incident on the VONA website. The time of the event was selected based on VONA observations with significant eruption height information.

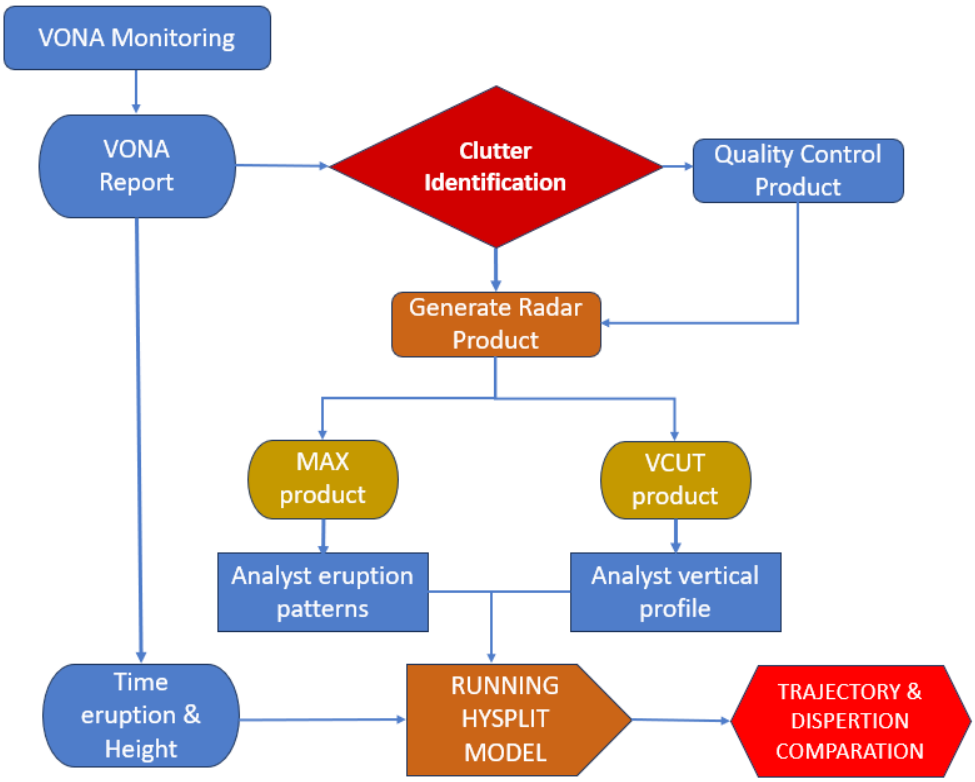

Figure 5. Flowchart of Radar Data Analysis and HYSPLIT Model to Identify Eruption Height and Volcanic Ash Distribution Direction

The radar products were processed within one hour before reporting to determine the existence of a precursor activity in the form of scattering volcanic ash prior to a major eruption. Volcanic ash scattered during the precursor activity was spread along with the eruption energy released by the volcano in the form of sulfur dioxide (SO_2) (Marshall et al., 2022) not directly observed through the eye.

The HYSPLIT model developed by the Air Resources Laboratory (ARL) and GDAS data from the NOAA database (NOAA, 2024) were used in this study to determine the direction of volcanic ash distribution immediately after the eruption (Hurst & Davis, 2017; Stein et al., 2015). The process included the simulations of the transport trajectories, dispersion, deposition of pollutants, and other hazardous materials in the atmosphere (Stein et al., 2015). Moreover, modelling was based on the Lagrangian equation of the horizontal movement of the pollutants or particles to determine the vertical movement of the terminal fall velocity (Tadini et al, 2020). The meteorological data from Global Data Assimilation System (GDAS) were used as the input in the HYSPLIT model (Crawford et al., 2022; Stein et al., 2015). These were in the form of the latitude and longitude of the volcano, the peak height, date and time of the eruption, the duration, the height of the ash column, and the level of ash reduction obtained from weather radar data processing.

The model parameters used were three height levels with the peak of Mount Sinabung recorded to be 2460 meters applied as the bottom level. Moreover, the results of weather radar eruption observation analysis were used as input for the top height level. Maximum (MAX) and VCUT (Vertical Cut) products from weather radar data processing were also adopted to obtain more detailed information on eruption activity with a focus on the eruption patterns and vertical profile analysis.

Analysis of Eruptive Activity based on MAX Reflectivity Products

Reflectivity pattern analysis was conducted by observing and interpreting radar images before and during the incident. The products were used to describe the patterns and characteristics of eruptions through the focus on the attributes of the echo at volcanic locations. Radar reflectivity intensity which was termed as the Z product was measured in decibels (dBZ) (Binetti et al., 2022). It was also observed that the eruption pattern was generally the same as the convective cloud precipitation with reflectivity values up to > 45 dBZ, depending on the scattering of material carried during the eruption. Meanwhile, the eruption pattern was differentiated from convective clouds in the cell growth phase. The observation image showed that the eruption pattern suddenly appeared as a matured convective cloud pattern without experiencing a growth phase, either through an increase in reflectivity values or cell area and height.

Vertical Eruption Profile Analysis

The vertical profile of volcanic eruption material was analyzed using the VCUT interactive products and tools. The information produced was used to describe the composition of eruptive materials from volcanic activity based on reflectivity values presented in Table 1.

3. Results and Discussion

Medan Weather Radar Observations During the Eruption of Mount Sinabung

The incident information from VONA observations were subjected to radar data processing with due consideration for similarity in date and time as presented in Table 2. The clutter identification at the location of Mount Sinabung showed that

no echo clutter could interfere with radar image analysis process during the eruption. Therefore, radar data QC process was not conducted and the CMAX and VCUT products were manufactured. Medan weather radar images were processed one hour before the time of reporting the eruption to determine the possible existence of any precursor activity not observed or recorded in the seismograph sensor.

a. The eruption of Mount Sinabung on July 28, 2021

The VONA information showed that Mount Sinabung eruption activity occurred on July 28 2021 at 06.20 UTC (13.20 West Indonesia Time) with a height of up to 4500 meters from the top of the mountain and volcanic ash was distributed in the East - South direction. Weather radar data of July 28 2021 processed in Figure 6 showed that the observation of volcanic activity of Mount Sinabung was initiated at 06.10 UTC (13.10 West Indonesia Time) and stopped at 06.40 UTC (13.40 West Indonesia Time). Moreover, the MAX height was up to 7900 meters which occurred at 06.40 UTC (13.40 West Indonesia Time).

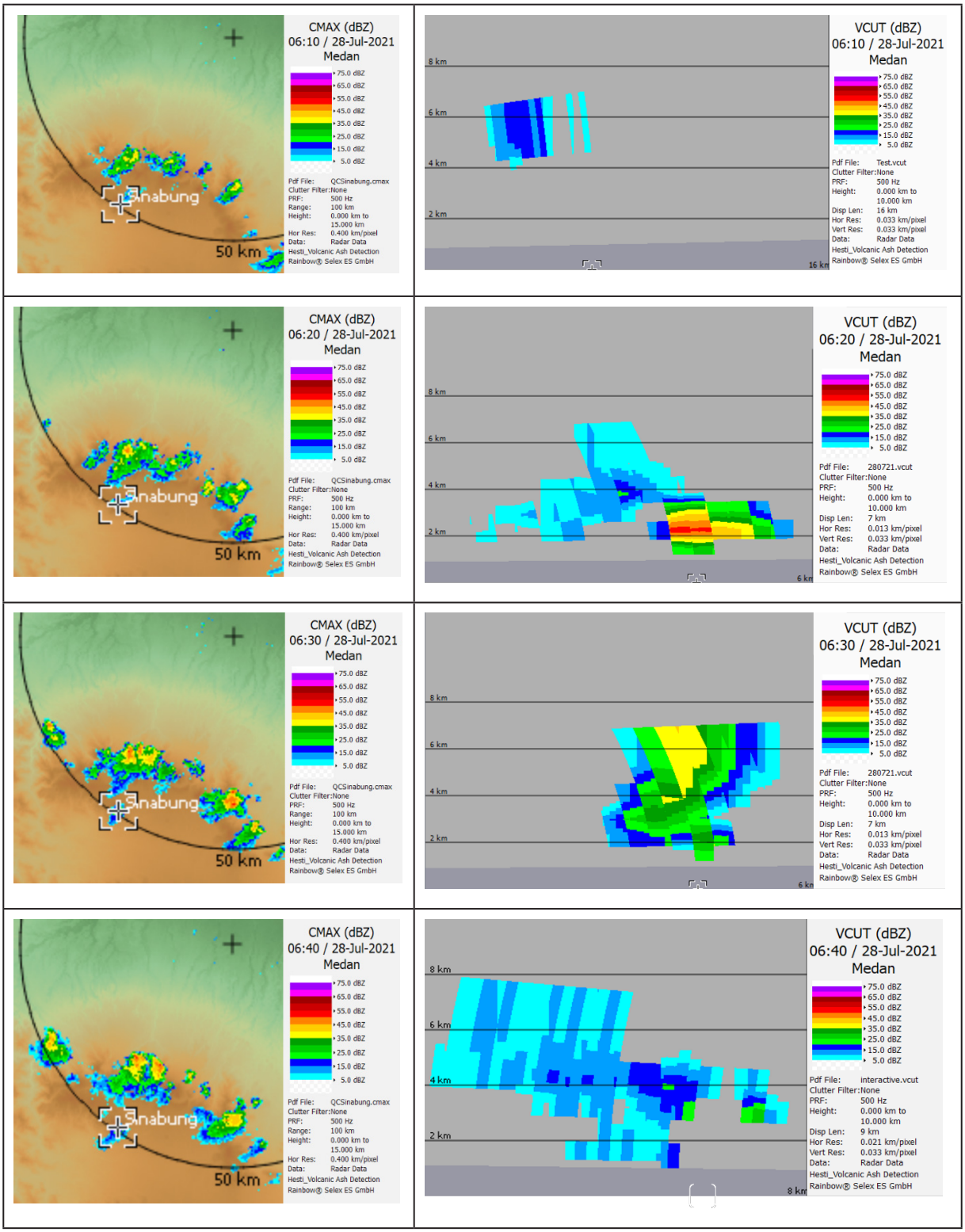

Figure 6. CMAX and VCUT products observations on July 28, 2021 at 06.10 UTC – 06.40 UTC

The HYSPLIT model on July 28 2021 showed the movement of volcanic ash in the Northeast - Southeast direction from the peak of Mount Sinabung as presented in Figure 7 (a).

There was a VONA report that an eruption of Mount Sinabung occurred at 02.08 UTC (09.08 West Indonesia Time) with a height of up to 2000 meters on May 7 2021. It was also reported that volcanic ash spread to the East at 08.19 UTC (15.19 West Indonesia Time) with an eruption height up to 3800 meters towards the North East – East as presented in Figure 7 (b).

b. The eruption of Mount Sinabung on May 7, 2021

Figure 8 shows an analysis of weather radar data processing of Mount Sinabung activity at 02.10 UTC (09.10 West Indonesia Time) with the height of volcanic ash distribution observed to be up to 4570 meters. The activity was again monitored from 08.20 UTC (15.20 West Indonesia Time) to 10.10 UTC (17.10 West Indonesia Time) with the MAX height of volcanic ash scattering up to approximately 10,000 meters at 10.00 UTC (17.00 West Indonesia Time).

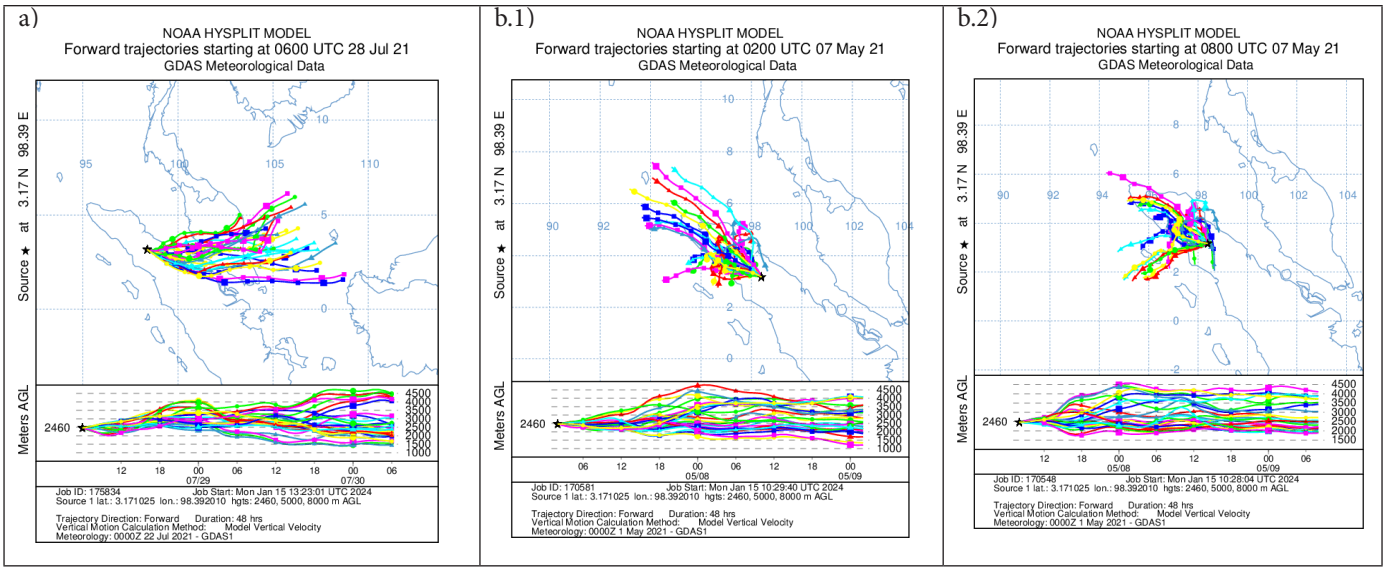

Figure 7. NOAA HYSPLIT model on July 28, 2021 at 06.00 UTC and May 7, 2021 at 02.00 UTC and 08.00 UTC

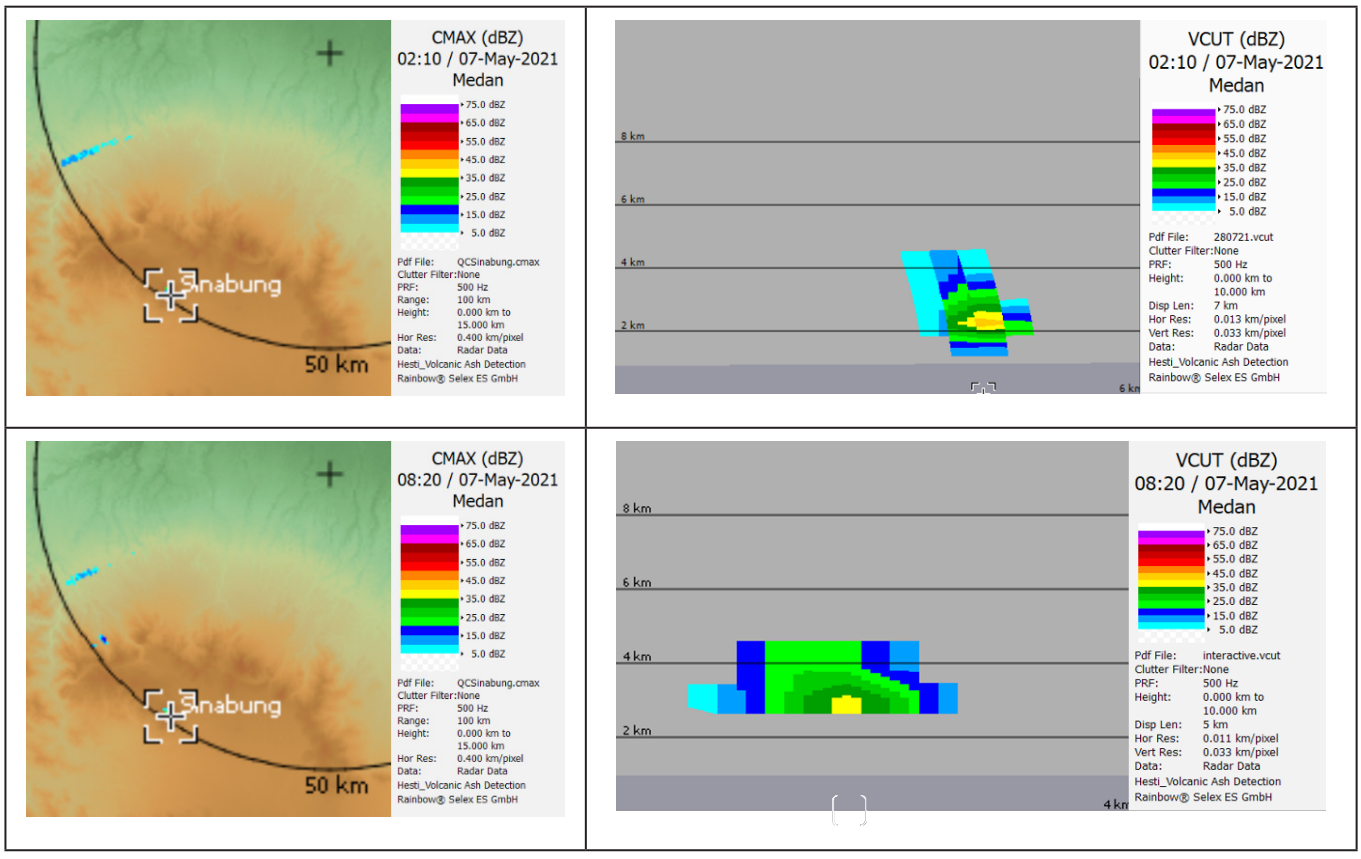

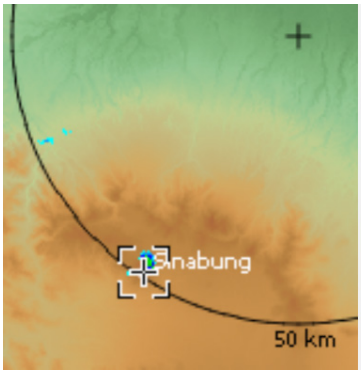
CMAX (dBZ)
08:30 / 07-May-2021
Medan
75.0 dBZ
65.0 dBZ
55.0 dBZ
45.0 dBZ
35.0 dBZ
25.0 dBZ
15.0 dBZ
5.0 dBZ
Pdf File: QCSinabung.cmax
Clutter Filter:None
PRF: 500 Hz
Range: 100 km
Height: 0.000 km to 15.000 km
Hor Res: 0.400 km/pixel
Data: Radar Data
Hesti_Volcanic Ash Detection
Rainbow® Selex ES GmbH
50 km

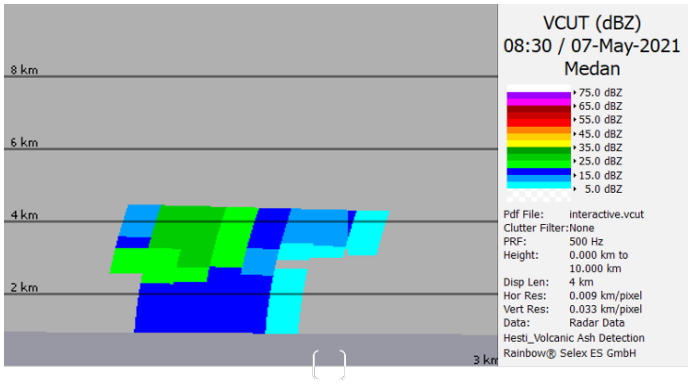
VCUT (dBZ)
08:30 / 07-May-2021
Medan
8 km
6 km
4 km
2 km
3 km
75.0 dBZ
65.0 dBZ
55.0 dBZ
45.0 dBZ
35.0 dBZ
25.0 dBZ
15.0 dBZ
5.0 dBZ
Pdf File: interactive.vcut
Clutter Filter:None
PRF: 500 Hz
Height: 0.000 km to 10.000 km
Disp Len: 4 km
Hor Res: 0.009 km/pixel
Vert Res: 0.033 km/pixel
Data: Radar Data
Hesti_Volcanic Ash Detection
Rainbow® Selex ES GmbH

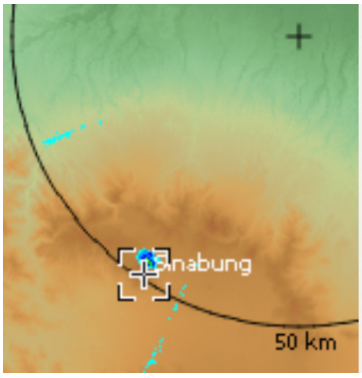
CMAX (dBZ)
08:40 / 07-May-2021
Medan
75.0 dBZ
65.0 dBZ
55.0 dBZ
45.0 dBZ
35.0 dBZ
25.0 dBZ
15.0 dBZ
5.0 dBZ
Pdf File: QCSinabung.cmax
Clutter Filter:None
PRF: 500 Hz
Range: 100 km
Height: 0.000 km to 15.000 km
Hor Res: 0.400 km/pixel
Data: Radar Data
Hesti_Volcanic Ash Detection
Rainbow® Selex ES GmbH
50 km

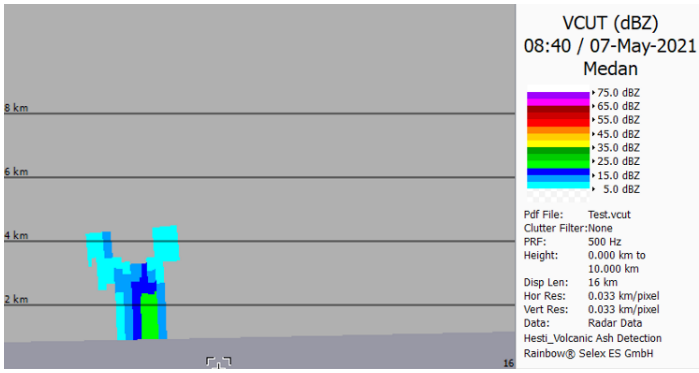
VCUT (dBZ)
08:40 / 07-May-2021
Medan
8 km
6 km
4 km
2 km
16
75.0 dBZ
65.0 dBZ
55.0 dBZ
45.0 dBZ
35.0 dBZ
25.0 dBZ
15.0 dBZ
5.0 dBZ
Pdf File: Test.vcut
Clutter Filter:None
PRF: 500 Hz
Height: 0.000 km to 10.000 km
Disp Len: 16 km
Hor Res: 0.033 km/pixel
Vert Res: 0.033 km/pixel
Data: Radar Data
Hesti_Volcanic Ash Detection
Rainbow® Selex ES GmbH

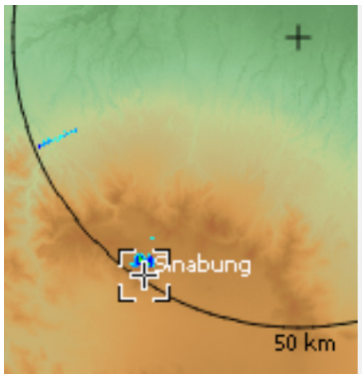
CMAX (dBZ)
08:50 / 07-May-2021
Medan
75.0 dBZ
65.0 dBZ
55.0 dBZ
45.0 dBZ
35.0 dBZ
25.0 dBZ
15.0 dBZ
5.0 dBZ
Pdf File: QCSinabung.cmax
Clutter Filter:None
PRF: 500 Hz
Range: 100 km
Height: 0.000 km to 15.000 km
Hor Res: 0.400 km/pixel
Data: Radar Data
Hesti_Volcanic Ash Detection
Rainbow® Selex ES GmbH
50 km

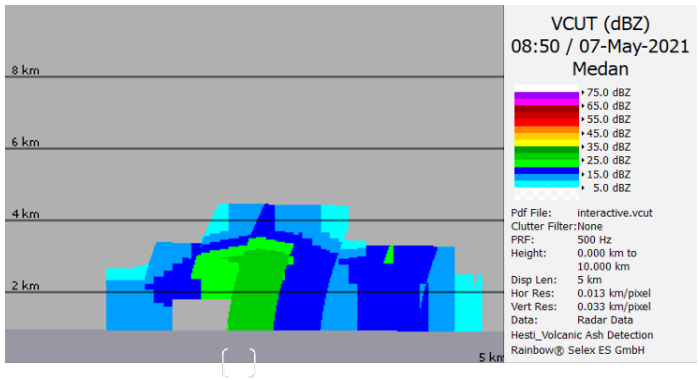
VCUT (dBZ)
08:50 / 07-May-2021
Medan
8 km
6 km
4 km
2 km
5 km
75.0 dBZ
65.0 dBZ
55.0 dBZ
45.0 dBZ
35.0 dBZ
25.0 dBZ
15.0 dBZ
5.0 dBZ
Pdf File: interactive.vcut
Clutter Filter:None
PRF: 500 Hz
Height: 0.000 km to 10.000 km
Disp Len: 5 km
Hor Res: 0.013 km/pixel
Vert Res: 0.033 km/pixel
Data: Radar Data
Hesti_Volcanic Ash Detection
Rainbow® Selex ES GmbH

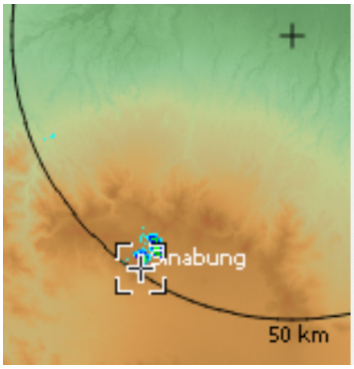
CMAX (dBZ)
09:00 / 07-May-2021
Medan
75.0 dBZ
65.0 dBZ
55.0 dBZ
45.0 dBZ
35.0 dBZ
25.0 dBZ
15.0 dBZ
5.0 dBZ
Pdf File: QCSinabung.cmax
Clutter Filter:None
PRF: 500 Hz
Range: 100 km
Height: 0.000 km to 15.000 km
Hor Res: 0.400 km/pixel
Data: Radar Data
Hesti_Volcanic Ash Detection
Rainbow® Selex ES GmbH
50 km

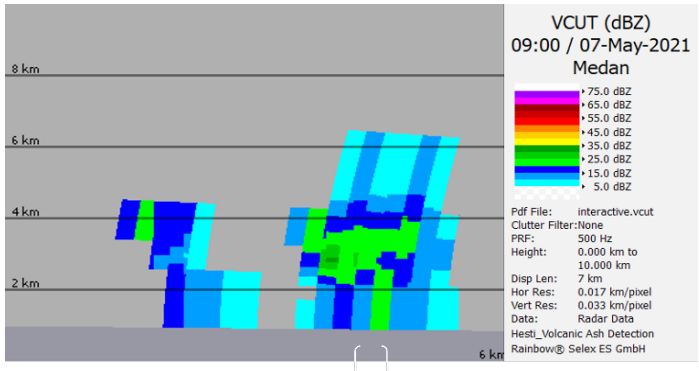
VCUT (dBZ)
09:00 / 07-May-2021
Medan
8 km
6 km
4 km
2 km
6 km
75.0 dBZ
65.0 dBZ
55.0 dBZ
45.0 dBZ
35.0 dBZ
25.0 dBZ
15.0 dBZ
5.0 dBZ
Pdf File: interactive.vcut
Clutter Filter:None
PRF: 500 Hz
Height: 0.000 km to 10.000 km
Disp Len: 7 km
Hor Res: 0.017 km/pixel
Vert Res: 0.033 km/pixel
Data: Radar Data
Hesti_Volcanic Ash Detection
Rainbow® Selex ES GmbH

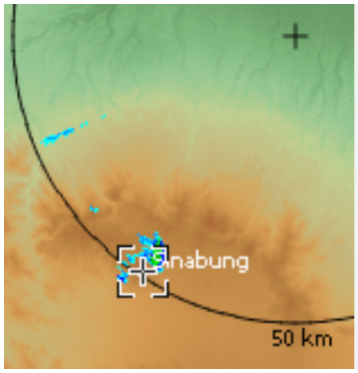
CMAX (dBZ)
09:10 / 07-May-2021
Medan
75.0 dBZ
65.0 dBZ
55.0 dBZ
45.0 dBZ
35.0 dBZ
25.0 dBZ
15.0 dBZ
5.0 dBZ
Pdf File: QCSinabung.cmax
Clutter Filter:None
PRF: 500 Hz
Range: 100 km
Height: 0.000 km to 15.000 km
Hor Res: 0.400 km/pixel
Data: Radar Data
Hesti_Volcanic Ash Detection
Rainbow® Selex ES GmbH
50 km

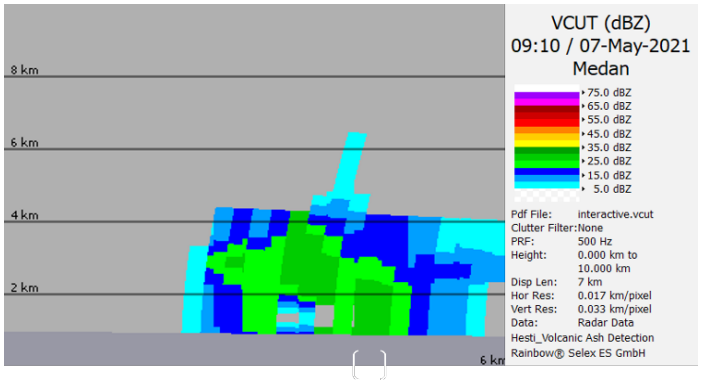
VCUT (dBZ)
09:10 / 07-May-2021
Medan
8 km
6 km
4 km
2 km
6 km
75.0 dBZ
65.0 dBZ
55.0 dBZ
45.0 dBZ
35.0 dBZ
25.0 dBZ
15.0 dBZ
5.0 dBZ
Pdf File: interactive.vcut
Clutter Filter:None
PRF: 500 Hz
Height: 0.000 km to 10.000 km
Disp Len: 7 km
Hor Res: 0.017 km/pixel
Vert Res: 0.033 km/pixel
Data: Radar Data
Hesti_Volcanic Ash Detection
Rainbow® Selex ES GmbH

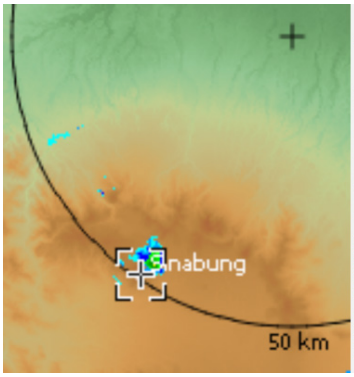

CMAX (dBZ)
09:20 / 07-May-2021
Medan

75.0 dBZ
65.0 dBZ
55.0 dBZ
45.0 dBZ
35.0 dBZ
25.0 dBZ
15.0 dBZ
5.0 dBZ

Pdf File: QCSinabung.cmax
Clutter Filter:None
PRF: 500 Hz
Range: 100 km
Height: 0.000 km to 15.000 km
Hor Res: 0.400 km/pixel
Data: Radar Data
Hesti_Volcanic Ash Detection
Rainbow® Selex ES GmbH

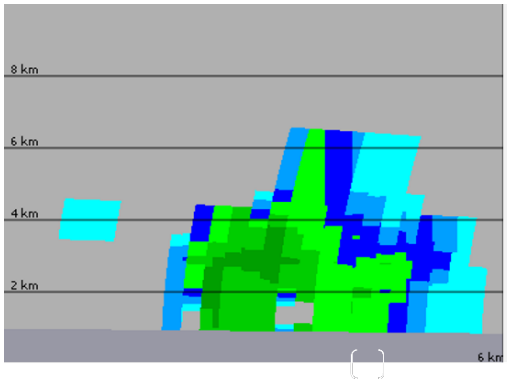

VCUT (dBZ)
09:20 / 07-May-2021
Medan

75.0 dBZ
65.0 dBZ
55.0 dBZ
45.0 dBZ
35.0 dBZ
25.0 dBZ
15.0 dBZ
5.0 dBZ

Pdf File: interactive.vcut
Clutter Filter:None
PRF: 500 Hz
Height: 0.000 km to 10.000 km
Disp Len: 7 km
Hor Res: 0.017 km/pixel
Vert Res: 0.033 km/pixel
Data: Radar Data
Hesti_Volcanic Ash Detection
Rainbow® Selex ES GmbH

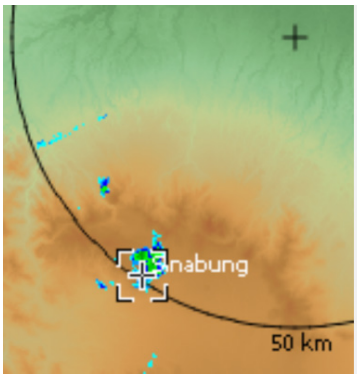

CMAX (dBZ)
09:30 / 07-May-2021
Medan

75.0 dBZ
65.0 dBZ
55.0 dBZ
45.0 dBZ
35.0 dBZ
25.0 dBZ
15.0 dBZ
5.0 dBZ

Pdf File: QCSinabung.cmax
Clutter Filter:None
PRF: 500 Hz
Range: 100 km
Height: 0.000 km to 15.000 km
Hor Res: 0.400 km/pixel
Data: Radar Data
Hesti_Volcanic Ash Detection
Rainbow® Selex ES GmbH

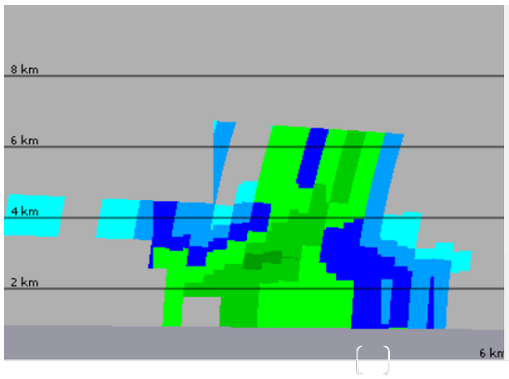

VCUT (dBZ)
09:30 / 07-May-2021
Medan

75.0 dBZ
65.0 dBZ
55.0 dBZ
45.0 dBZ
35.0 dBZ
25.0 dBZ
15.0 dBZ
5.0 dBZ

Pdf File: interactive.vcut
Clutter Filter:None
PRF: 500 Hz
Height: 0.000 km to 10.000 km
Disp Len: 7 km
Hor Res: 0.017 km/pixel
Vert Res: 0.033 km/pixel
Data: Radar Data
Hesti_Volcanic Ash Detection
Rainbow® Selex ES GmbH

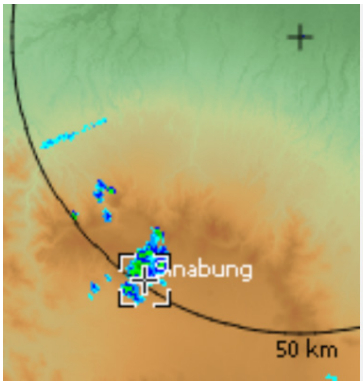

CMAX (dBZ)
09:40 / 07-May-2021
Medan

75.0 dBZ
65.0 dBZ
55.0 dBZ
45.0 dBZ
35.0 dBZ
25.0 dBZ
15.0 dBZ
5.0 dBZ

Pdf File: QCSinabung.cmax
Clutter Filter:None
PRF: 500 Hz
Range: 100 km
Height: 0.000 km to 15.000 km
Hor Res: 0.400 km/pixel
Data: Radar Data
Hesti_Volcanic Ash Detection
Rainbow® Selex ES GmbH

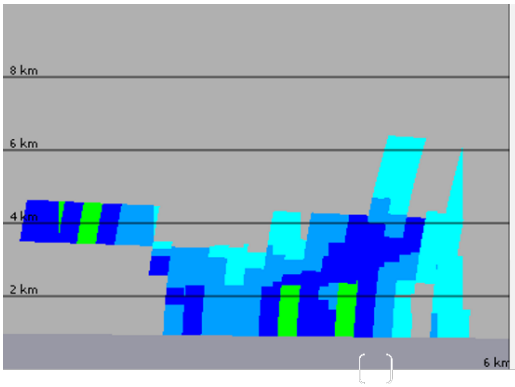

VCUT (dBZ)
09:40 / 07-May-2021
Medan

75.0 dBZ
65.0 dBZ
55.0 dBZ
45.0 dBZ
35.0 dBZ
25.0 dBZ
15.0 dBZ
5.0 dBZ

Pdf File: interactive.vcut
Clutter Filter:None
PRF: 500 Hz
Height: 0.000 km to 10.000 km
Disp Len: 7 km
Hor Res: 0.017 km/pixel
Vert Res: 0.033 km/pixel
Data: Radar Data
Hesti_Volcanic Ash Detection
Rainbow® Selex ES GmbH

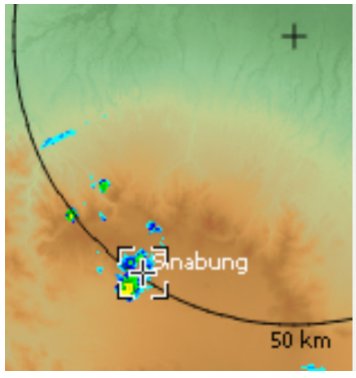

CMAX (dBZ)
09:50 / 07-May-2021
Medan

75.0 dBZ
65.0 dBZ
55.0 dBZ
45.0 dBZ
35.0 dBZ
25.0 dBZ
15.0 dBZ
5.0 dBZ

Pdf File: QCSinabung.cmax
Clutter Filter:None
PRF: 500 Hz
Range: 100 km
Height: 0.000 km to 15.000 km
Hor Res: 0.400 km/pixel
Data: Radar Data
Hesti_Volcanic Ash Detection
Rainbow® Selex ES GmbH

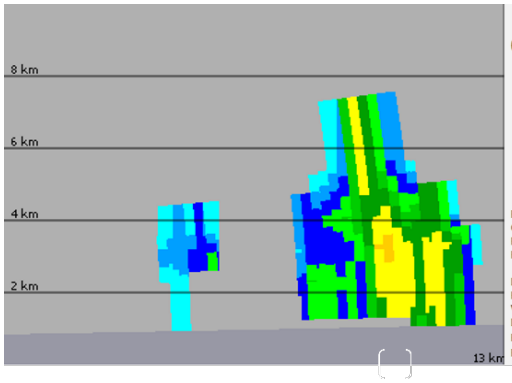

VCUT (dBZ)
09:50 / 07-May-2021
Medan

75.0 dBZ
65.0 dBZ
55.0 dBZ
45.0 dBZ
35.0 dBZ
25.0 dBZ
15.0 dBZ
5.0 dBZ

Pdf File: interactive.vcut
Clutter Filter:None
PRF: 500 Hz
Height: 0.000 km to 10.000 km
Disp Len: 13 km
Hor Res: 0.033 km/pixel
Vert Res: 0.033 km/pixel
Data: Radar Data
Hesti_Volcanic Ash Detection
Rainbow® Selex ES GmbH

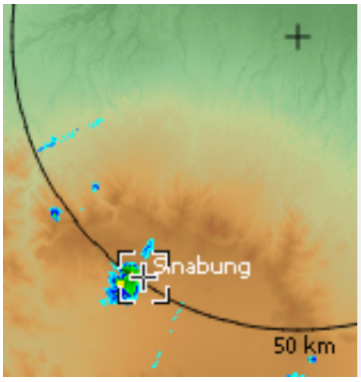

CMAX (dBZ)
10:00 / 07-May-2021
Medan

75.0 dBZ
65.0 dBZ
55.0 dBZ
45.0 dBZ
35.0 dBZ
25.0 dBZ
15.0 dBZ
5.0 dBZ

Pdf File: QCSinabung.cmax
Clutter Filter:None
PRF: 500 Hz
Range: 100 km
Height: 0.000 km to 15.000 km
Hor Res: 0.400 km/pixel
Data: Radar Data
Hesti_Volcanic Ash Detection
Rainbow® Selex ES GmbH

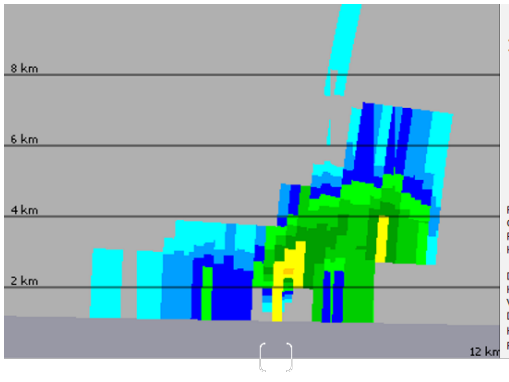

VCUT (dBZ)
10:00 / 07-May-2021
Medan

75.0 dBZ
65.0 dBZ
55.0 dBZ
45.0 dBZ
35.0 dBZ
25.0 dBZ
15.0 dBZ
5.0 dBZ

Pdf File: interactive.vcut
Clutter Filter:None
PRF: 500 Hz
Height: 0.000 km to 10.000 km
Disp Len: 12 km
Hor Res: 0.031 km/pixel
Vert Res: 0.033 km/pixel
Data: Radar Data
Hesti_Volcanic Ash Detection
Rainbow® Selex ES GmbH

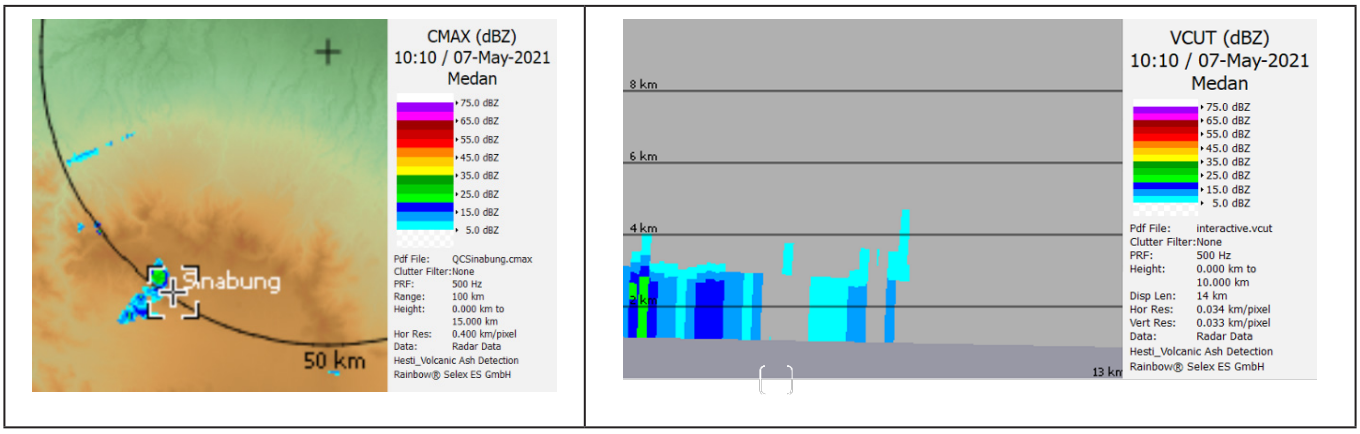

Figure 8. CMAX and VCUT products observations on May 7, 2021 at 02.10 UTC, 08.20 UTC, 09.00 UTC, and 09.30 UTC – 10.10 UTC

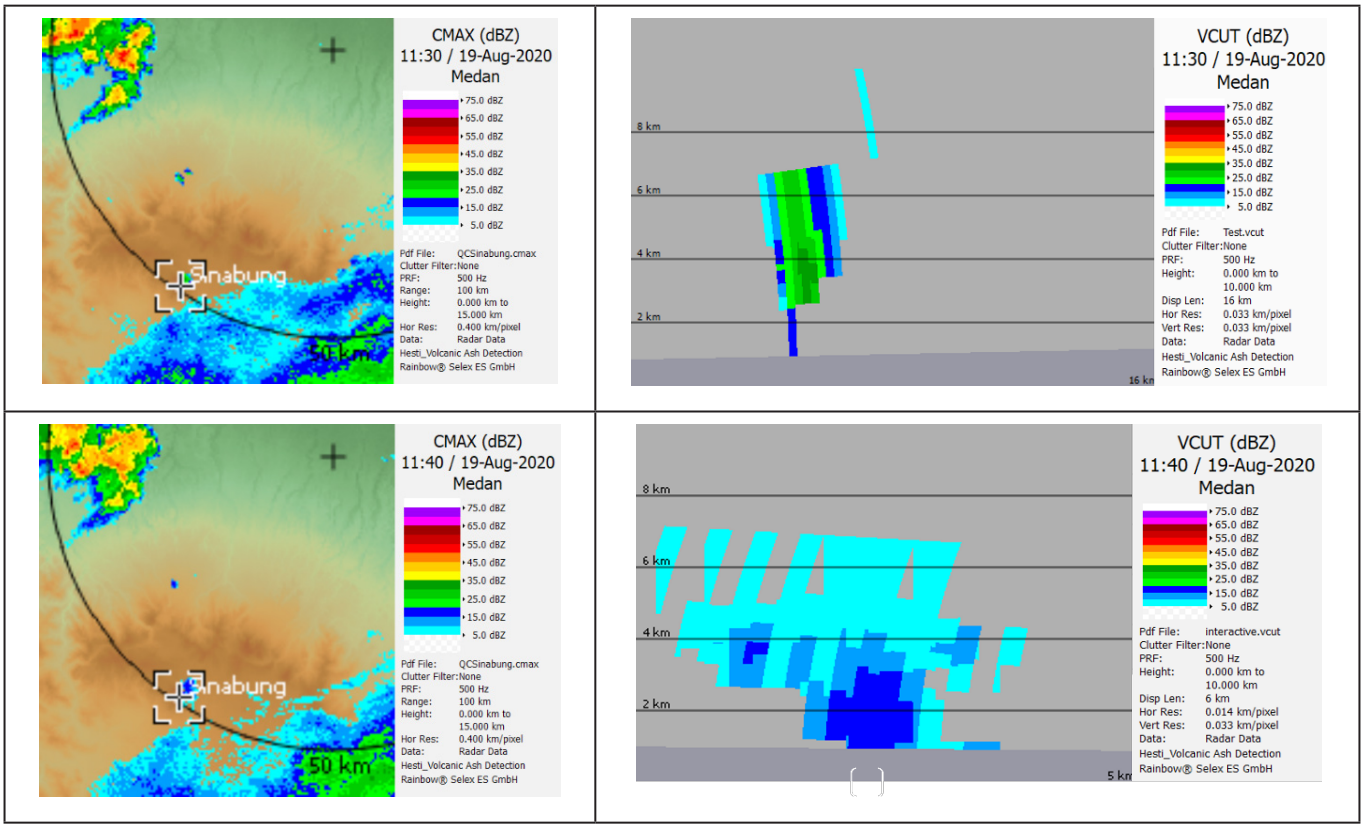

Figure 9. CMAX and VCUT products observations on August 19, 2020

The HYSPLIT model results related to the observation on May 7 2021 at 02.00 UTC and 08.00 UTC are presented in Figures 7 (b.1) and (b.2). Both models showed that the distribution was towards the Southwest–Northwest from the peak of Mount Sinabung.

c. The eruption of Mount Sinabung on August 19, 2020

The VONA observations on August 19 2020 showed an eruption of Mount Sinabung at 11.23 UTC (18.23 West Indonesia Time) with a height of up to 4000 meters. The distribution of volcanic ash was also in the East – Southeast direction.

The analysis of weather radar data showed that there was no eruption during observations at 11.20 UTC (18.20 West Indonesia Time). However, activity was observed at 11.30 and 11.40 UTC (18.30 and 18.40 West Indonesia Time) with volcanic ash scattering up to heights of 7000 meters and 7130 meters as presented in Figure 9.

Figure 10 (a) shows the results of the HYSPLIT model for the eruption of Mount Sinabung on 19 August 2020 at 11.00 UTC (18.00 West Indonesia Time). It was observed that volcanic ash distribution moved towards the North – Northeast direction.

d. The eruption of Mount Sinabung on August 14, 2020

The VONA report recorded two eruptions on August 14 2020 and the first was at 03.30 UTC (10.30 West Indonesia Time) with a height estimated to be 2100 meters and volcanic ash spread to the Southeast – South direction. The second was at 09.56 UTC (16.56 West Indonesia Time) with the height of the eruption column reaching approximately 4200 meters and volcanic ash spread to the East direction.

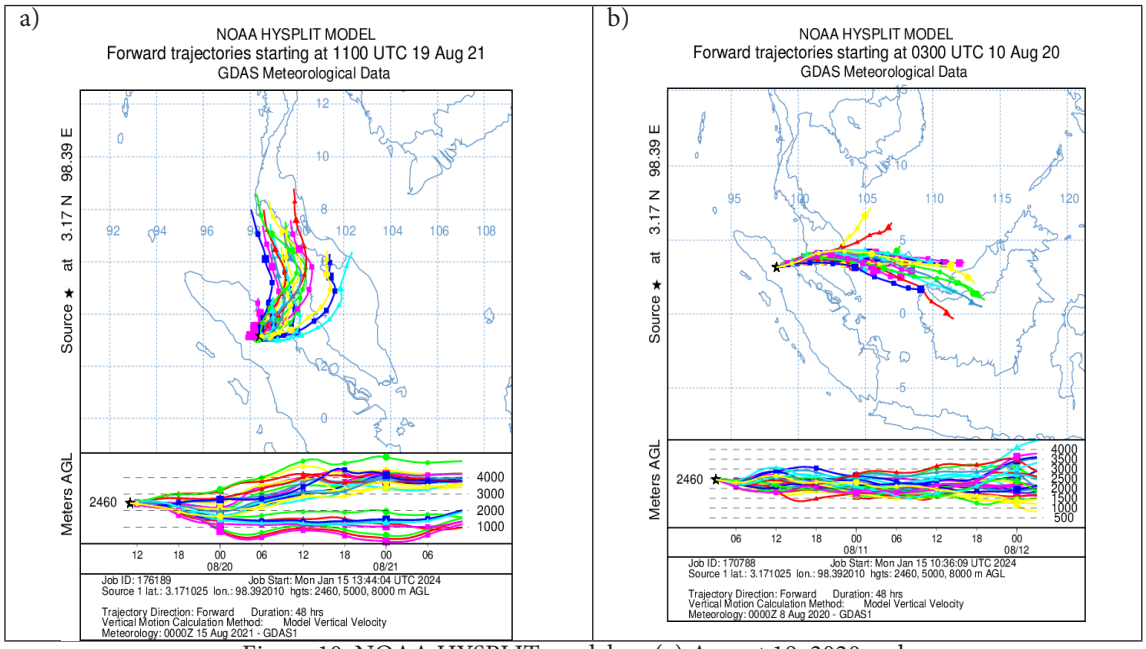

Figure 10. NOAA HYSPLIT model on (a) August 19, 2020 and (b) August 10, 2020

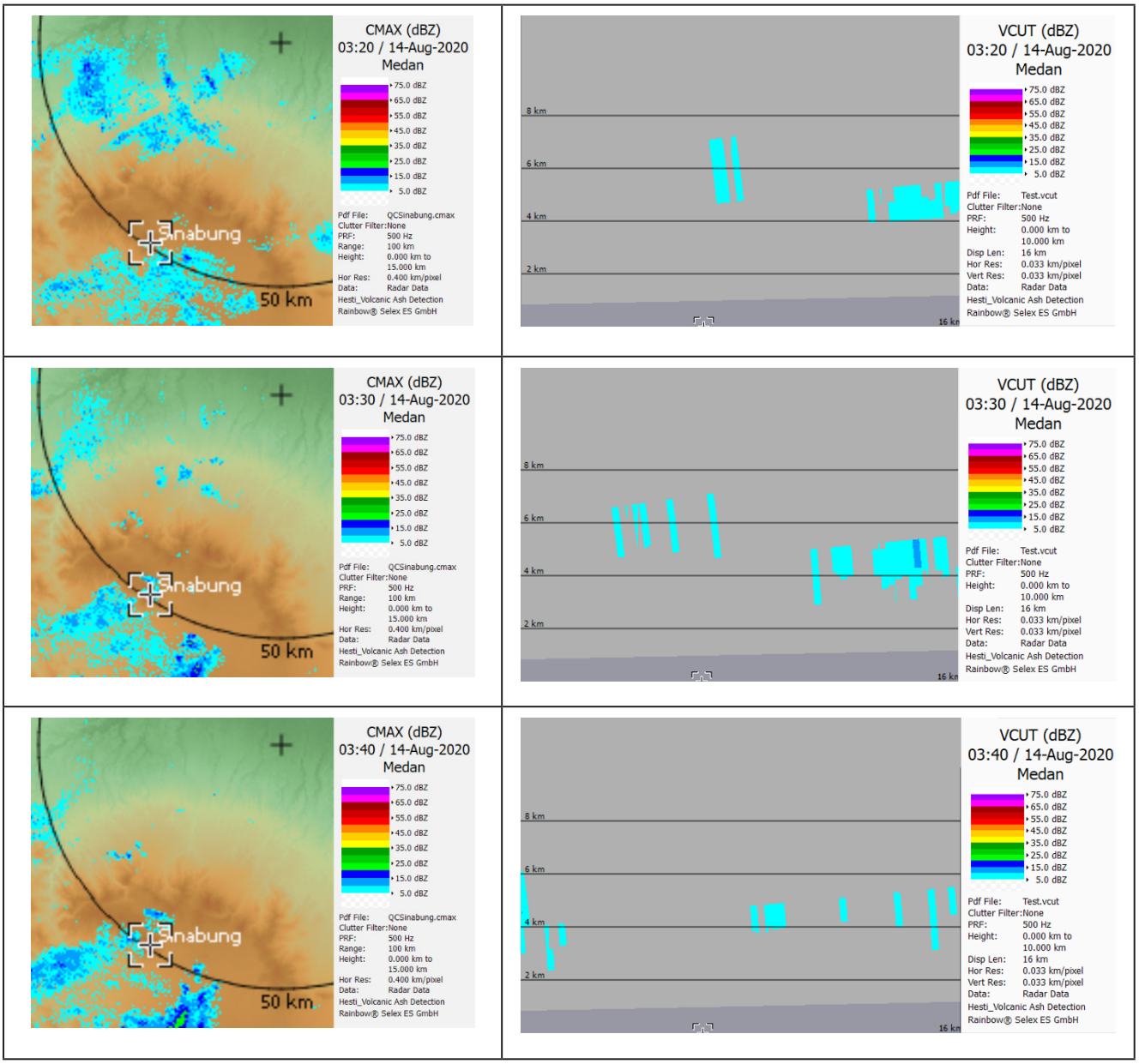

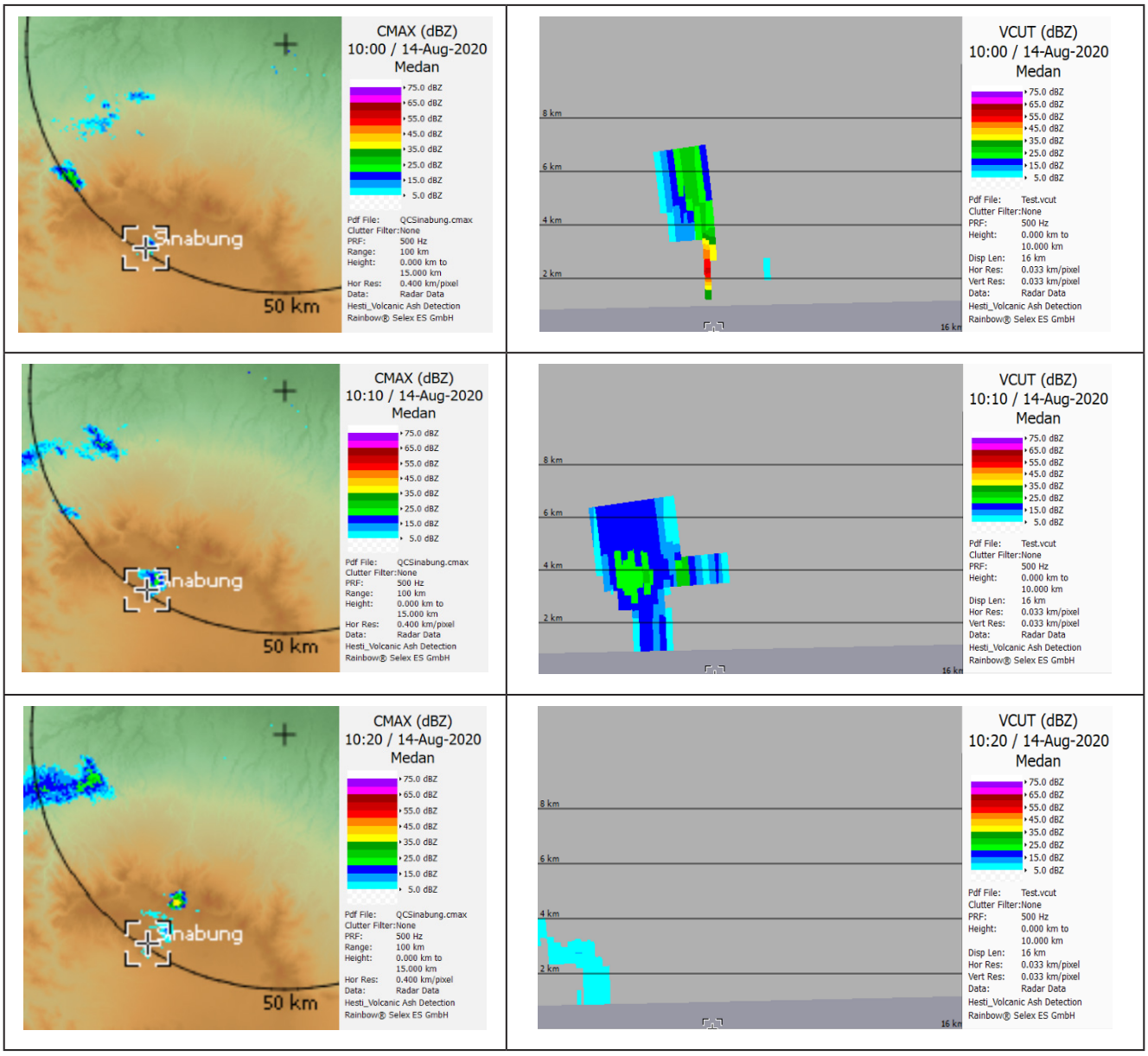

Figure 11. CMAX and VCUT products observations on August 14, 2020

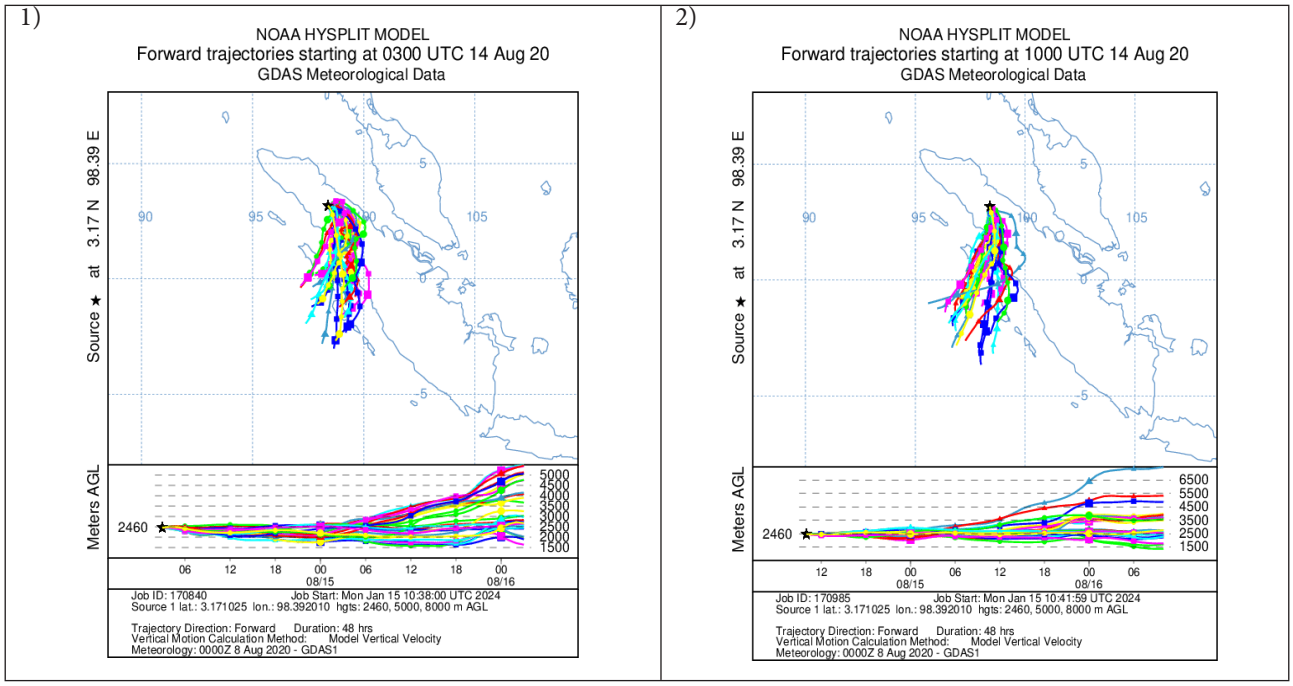

Figure 12. NOAA HYSPLIT model on August 14, 2020

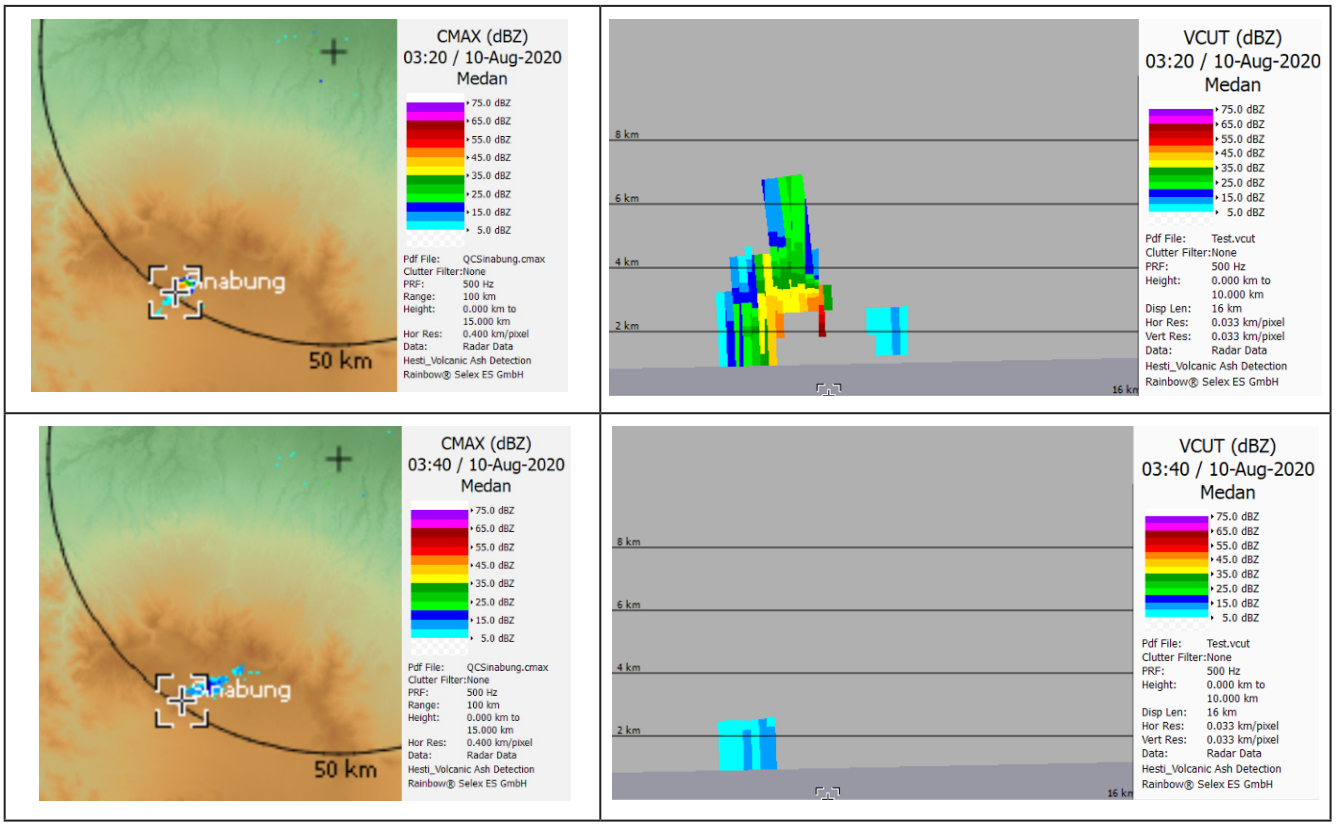

Figure 13. CMAX and VCUT products observations on August 10, 2020

The analysis of weather radar data processing showed there was insignificant volcanic activity from 03.20 UTC (10.20 West Indonesia Time) to 03.40 UTC (10.30 West Indonesia Time). Meanwhile, the observations at 10.00 UTC (17.00 West Indonesia Time) recorded significant eruptive activity with volcanic ash scattering up to a height of 7000 meters. The activity was still visible up to 10.20 UTC (17.20 West Indonesia Time) as shown in Figure 11.

The HYSPLIT Model results for the eruption on 14 August 2020 at 03.00 UTC (10.00 West Indonesia Time) and 10.00 UTC (17.00 West Indonesia Time) are presented in Figures 12 (1) and (2). It was observed that the movement of volcanic ash was in the South–Southwest direction.

f. The eruption of Mount Sinabung on August 10, 2020

The activity on August 10 2020 was reported by VONA to have occurred at 03.16 UTC (10.16 West Indonesia Time) with an eruption height of up to 5000 meters and volcanic ash was distributed in the East – Southeast direction. Moreover, the results of weather radar observations in Figure 13 show a significant activity at 03.20 UTC (10.20 West Indonesia Time) up to 03.40 UTC (10.40 West Indonesia Time). The MAX eruption column height was observed to be up to 7000 meters. The results of the HYSPLIT Model for the eruption on August 10 2020 at 03.00 UTC (10.00 West Indonesia Time) showed that volcanic ash moved in the Northeast–Southeast direction as presented in Figure 10 (b).

4. Conclusion

In conclusion, the analysis of the Mount Sinabung eruption showed a difference in the heights of the eruption activities based on weather radar data processing and the VONA observation reports conducted visually. The results in Table 2 showed that the average values obtained for height in weather radar observation data processing were much higher than the VONA observation report and the duration of the eruption was presented in more detail. Moreover, weather radar observation comprehensively identified volcanic activities in the pre- and post-eruption stages with more detail on volcanic ash material scattered through blowing or eruptions. The trend was due to the ability of radar to directly detect the materials scattered in eruption cloud structures, including those visible to the naked eye and particles with very small sizes as classified by Marzano et.al (2013) in Table 1.

The NOAA HYSPLIT model used weather radar observations as input to analyze volcanic ash trajectories and dispersion. The results showed different volcanic ash dispersion directions compared to the VONA observation input. It was observed that weather radar observation products reflected the actual volcanic ash dispersion conditions better. The results of altitude analysis conducted using weather radar could be used as input for volcanic ash trajectory and dispersion models such as HYSPLIT, Puff, Numerical Atmospheric-dispersion Modelling Environment (NAME), and others to produce more accurate information.

Acknowledgement

References

1. Ali, Abdullah & Umam, Iddam Hairuly & Argo, Henrikus Jatining Wahyu & Argo, Wahyu & Haryadi, & Permana, Deni & Deranadyan, Gumilang & Adiyasa, Alif & Winata, Nanda. (2023). SIDARMA: Web-GIS and Android Application-Based In-House Weather Radar Integration System. GEOMATICS. 29. 1-8

2. Aliotta, L., Gigante, V., & Lazzeri, A. (2023). Volcanic ash as filler in biocomposites: An example of circular economy in volcanic areas. Sustainable Materials and Technologies, 37(June), e00660. https://doi.org/10.1016/j.susmat.2023.e00660
3. Ariyanti, V., Gaafar, T., De La Sala, S., Edelenbos, J., & Scholten, P. (2020). Towards liveable volcanic cities: A look at the governance of lahars in Yogyakarta, Indonesia, and Latacunga, Ecuador. Cities, 107(July), 102893. https://doi.org/10.1016/j.cities.2020.102893
4. Binetti, M.S., Campanale, C., Massarelli, C., & Uricchio, V.F. (2022). The Use of Weather Radar Data: Possibilities, Challenges and Advanced Applications. Earth (Switzerland), 3(1), 157–171. https://doi.org/10.3390/earth3010012
5. Black, B.A., Lamarque, J.F., Marsh, D.R., Schmidt, A., & Bardeen, C.G. (2021). Global climate disruption and regional climate shelters after the Toba supereruption. Proceedings of the National Academy of Sciences of the United States of America, 118(29), 1–8. https://doi.org/10.1073/pnas.2013046118
6. Cahalan, R.C., Mastin, L.G., Van Eaton, A.R., Hurwitz, S., Smith, A.B., Dufek, J., Solovitz, S.A., Patrick, M., Schmith, J., Parcheta, C., Thelen, W.A., & Downs, D.T. (2023). Dynamics of the December 2020 Ash-Poor Plume Formed by Lava-Water Interaction at the Summit of Kīlauea Volcano, Hawai' i. Geochemistry, Geophysics, Geosystems, 24(3), 1–23. https://doi.org/10.1029/2022GC010718
7. Carlsen, H.K., Aspelund, T., Briem, H., Gislason, T., Jóhannsson, T., Valdimarsdóttir, U., & Gudnason, T. (2019). Respiratory health among professionals exposed to extreme SO2 levels from a volcanic eruption. Scandinavian Journal of Work, Environment and Health, 45(3), 312–315. https://doi.org/10.5271/sjweh.3783
8. Crawford, A., Chai, T., Wang, B., Ring, A., Studer, B., Loughner, C. P., Pavolonis, M., & Sieglaff, J. (2022). Evaluation and bias correction of probabilistic volcanic ash forecasts. Atmospheric Chemistry and Physics, 22(21), 13967–13996. https://doi.org/10.5194/acp-22-13967-2022
9. Durant, A. J., Bonadonna, C., & Horwell, C. J. (2010). Atmospheric and environmental impacts of volcanic particulates. Elements, 6(4), 235–240. https://doi.org/10.2113/gselements.6.4.235
10. Engwell, S., Mastin, L., Tupper, A., Kibler, J., Acethorp, P., Lord, G., & Filgueira, R. (2021). Near-real-time volcanic cloud monitoring: insights into global explosive volcanic eruptive activity through analysis of Volcanic Ash Advisories. Bulletin of Volcanology, 83(2). https://doi.org/10.1007/s00445-020-01419-y
11. Falconi, M.T., & Marzano, F.S. (2019). Weather Radar Data Processing and Atmospheric Applications. June, 85–97.
12. Hapsari, RI, Sugna, BAI, Novianto, D., Asmara, RA, & Oishi, S. (2020). Naïve Bayes Classifier for Debris Flow Disaster Mitigation in Mount Merapi Volcanic Rivers, Indonesia, Using X-band Polarimetric Radar. International Journal of Disaster Risk Science, 11(6), 776–789. https://doi.org/10.1007/s13753-020-00321-7
13. Hirtl, M., Arnold, D., Baro, R., Brenot, H., Coltelli, M., Eschbacher, K., Hard-Stremayer, H., Lipok, F., Maurer, C., Meinhard, D., Mona, L., D. Mulder, M., Papagiannopoulos, N., Pernsteiner, M., Plu, M., Robertson, L., Roki, K., Schellin-Pirscher, B., Sievers, K., … Zopp, R. (2020). A volcanic-hazard demonstration exercise to assess and mitigate the impacts of volcanic ash clouds on civil and military aviation. Natural Hazards and Earth System Sciences, 20(6), 1719–1739. https://doi.org/10.5194/nhess-20-1719-2020
14. Hurst, T., & Davis, C. (2017). Forecasting volcanic ash deposition using HYSPLIT. https://doi.org/10.1186/s13617-017-0056-7
15. Irwandi, I., Ilhamsyah, Y., Permana, D. S., Haloho, M. P., Prasetyo, B., & Dana, I. N. (2019). Application of C-band Doppler Weather Radar (CDR) for Detecting Volcanic Ash Dispersion of Sinabung Eruption 19 February 2018. IOP Conference Series: Earth and Environmental Science, 273(1). https://doi.org/10.1088/1755-1315/273/1/012019
16. Ministry of Energy and Mineral Resources (2023). Types of Volcanoes in Indonesia (A, B, and C).https://magma.esdm.go.id/v1/edukasi/tipe-gunung-api-di-indonesia-ab-dan-c. Retrieved December 8, 2023.
17. Ministry of Energy and Mineral Resources (2024). VONA Archived.https://magma.esdm.go.id/v1/vona?code=SIN. Retrieved January 14, 2024.
18. Ministry of Energy and Mineral Resources (2024). Press Release DEVELOPMENT OF SINABUNG VOLCANO ACTIVITIES.https://vsi.esdm.go.id/press-release/press-release-perkembangan-angkat-gunung-api-sinabung. Accessed 08 February 2024.
19. Maki, M., Kim, Y., Kobori, T., Hirano, K., Lee, D.I., & Iguchi, M. (2021). Analyzes of three-dimensional weather radar data from volcanic eruption clouds. Journal of Volcanology and Geothermal Research, 412. https://doi.org/10.1016/j.jvolgeores.2021.107178
20. Maki, M., Takaoka, R., & Iguchi, M. (2021). Characteristics of particle size distributions of falling volcanic ash measured by optical disdrometers at the Sakurajima volcano, Japan. Atmosphere, 12(5). https://doi.org/10.3390/atmos12050601
21. Marshall, L.R., Maters, E.C., Schmidt, A., Timmreck, C., Robock, A., & Toohey, M. (2022). Volcanic effects on climate: recent advances and future avenues. Bulletin of Volcanology, 84(5). https://doi.org/10.1007/s00445-022-01559-3
22. Marzano, F.S. (2011). Remote Sensing of Volcanic Ash Cloud During Explosive Eruptions. March, 0–3.
23. Marzano, F.S., Barbieri, S., Picciotti, E., & Vulpiani, G. (2007). Microwave radar remote sensing of Plinian volcanic ash clouds for aviation hazard and civil protection applications. International Geoscience and Remote Sensing Symposium (IGARSS). https://doi.org/10.1109/IGARSS.2007.4423658
24. Marzano, F.S., Barbieri, S., Vulpiani, G., & Rose, W.I. (2006). Volcanic ash cloud retrieval by ground-based microwave weather radar. IEEE Transactions on Geoscience and Remote Sensing, 44(11). https://doi.org/10.1109/TGRS.2006.879116
25. Marzano, F.S., Lamantea, M., Montopoli, M., Di Fabio, S., & Picciotti, E. (2011). The Eyjafjöll explosive volcanic eruption from a microwave weather radar perspective. Atmospheric Chemistry and Physics, 11(18). https://doi.org/10.5194/acp-11-9503-2011
26. Marzano, F.S., Lamantea, M., Montopoli, M., Herzog, M., Graf, H., & Cimini, D. (2013). Remote Sensing of Environment Microwave remote sensing of the 2011 Plinian eruption of the Grímsvötn Icelandic volcano. Remote Sensing of Environment, 129, 168–184. https://doi.org/10.1016/j.rse.2012.11.005
27. Marzano, F.S., Marchiotto, S., Textor, C., & Schneider, D.J. (2010). Model-based weather radar remote sensing of explosive volcanic ash eruption. IEEE Transactions on Geoscience and Remote Sensing, 48(10). https://doi.org/10.1109/TGRS.2010.2047862
28. Marzano, F.S., Picciotti, E., Montopoli, M., & Vulpiani, G. (2013). Inside volcanic clouds: Remote sensing of ash plumes using microwave weather radars. Bulletin of the American Meteorological Society, 94(10). https://doi.org/10.1175/BAMS-D-11-00160.1
29. Marzano, F.S., Vulpiani, G., & Rose, W.I. (2006). Microphysical characterisation of microwave radar reflectivity due to volcanic ash clouds. IEEE Transactions on Geoscience and Remote Sensing, 44(2), 313–327. https://doi.org/10.1109/TGRS.2005.861010
30. Nakada, S., Zaennudin, A., Yoshimoto, M., Maeno, F., Suzuki, Y., Hokanishi, N., Sasaki, H., Iguchi, M., Ohkura, T., Gunawan, H., & Triastuty, H. (2019). Growth process of the lava dome/flow complex at Sinabung Volcano during 2013–2016. Journal of

Volcanology and Geothermal Research, 382, 120–136. https://doi.org/10.1016/j.jvolgeores.2017.06.012

31. Nasruddin, Idrus Alhamid, M., Daud, Y., Surachman, A., Sugiyono, A., Aditya, HB, & Mahlia, TMI (2016). Potential of geothermal energy for electricity generation in Indonesia: A review. Renewable and Sustainable Energy Reviews, 53(2016), 733–740. https://doi.org/10.1016/j.rser.2015.09.032
32. NOAA Air Resources Laboratory. Available online: https://www.ready.noaa.gov/HYSPLIT.php (accessed 15 January 2024)
33. Osipov, S., Stenchikov, G., Tsigaridis, K., LeGrande, A.N., & Bauer, S.E. (2020). The Role of the SO 2 Radiative Effect in Sustaining the Volcanic Winter and Soothing the Toba Impact on Climate. Journal of Geophysical Research: Atmospheres, 125(2). https://doi.org/10.1029/2019JD031726
34. Paredes-Mariño, J., Forte, P., Alois, S., Chan, K.L., Cigala, V., Mueller, S.B., Poret, M., Spanu, A., Tomašek, I., Tournigand, P.Y., Perugini, D., & Kueppers, U. (2022). The lifecycle of volcanic ash: advances and ongoing challenges. Bulletin of Volcanology, 84(5). https://doi.org/10.1007/s00445-022-01557-5
35. Karo Regency Government (2023). http://pariwisata.karokab.go.id/up/index.php/en/besar-wisata/produk-wisata-alam/6-gunung-sinabung. Retrieved December 8, 2023.
36. Poland, M. P., Lopez, T., Wright, R., & Pavolonis, M. J. (2020). Forecasting, Detecting, and Tracking Volcanic Eruptions from Space. Remote Sensing in Earth Systems Sciences, 3(1–2), 55–94. https://doi.org/10.1007/s41976-020-00034-x
37. Poulidis, A.P., Shimizu, A., Nakamichi, H., & Iguchi, M. (2021). A computational methodology for the calibration of tephra transport nowcasting at Sakurajima volcano, Japan. Atmosphere, 12(1), 1–15. https://doi.org/10.3390/atmos12010104
38. Prata, F., Rose, B. (2015). Chapter 52: Volcanic Ash Hazards to Aviation. The Encyclopedia of Volcanoes (Second Edition), Pages 911-934. https://doi.org/10.1016/B978-0-12-385938-9.00052-3
39. Prata, F. (2020). Detection and avoidance of atmospheric aviation hazards using infrared spectroscopic imaging. Remote Sensing, 12(14), 1–31. https://doi.org/10.3390/rs12142309
40. Reichardt, U., Ulfarsson, G.F., & Pétursdóttir, G. (2019). Developing scenarios to explore impacts and weaknesses in aviation response exercises for volcanic ash eruptions in Europe. Journal of Air Transport Management, 79(June), 101684. https://doi.org/10.1016/j.jairtraman.2019.101684
41. Rizza, U., Donnadieu, F., Magazu, S., Passerini, G., Castorina, G., Semprebello, A., Morichetti, M., Virgili, S., & Mancinelli, E. (2021). Effects of variable eruption source parameters on volcanic plume transport: Example of the 23 November 2013 paroxysm of Etna. Remote Sensing, 13(20), 1–25. https://doi.org/10.3390/rs13204037
42. Sato, E. (2021). Kusatsu-Shirane volcano eruption on January 23, 2018, observed using JMA operational weather radars. Earth, Planets and Space, 73(1). https://doi.org/10.1186/s40623-021-01445-w
43. Sato, E., Fukui, K., & Shimbori, T. (2018). Aso volcano eruption on October 8, 2016, observed by weather radars. In Earth, Planets and Space (Vol. 70, Issue 1). https://doi.org/10.1186/s40623-018-0879-4
44. Sokol, Z., Szturc, J., Orellana-Alvear, J., Popová, J., Jurczyk, A., & Célleri, R. (2021). The role of weather radar in rainfall estimation and its application in meteorological and hydrological modeling —A review. Remote Sensing, 13(3), 1–38. https://doi.org/10.3390/rs13030351
45. Stein, A.F., Draxler, R.R., Rolph, G.D., Stunder, B.J.B., Cohen, M.D., & Ngan, F. (2015). Noaa's HYSPLIT atmospheric transport and dispersion modeling system. Bulletin of the American Meteorological Society, 96(12), 2059–2077. https://doi.org/10.1175/BAMS-D-14-00110.1
46. Tadini, A., Roche, O., Samaniego, P., Guillin, A., Azzaoui, N., Gouhier, M., … Le Pennec, J.L. (2020). Quantifying the Uncertainty of a Coupled Plume and Tephra Dispersal Model PLUME-MOM. Journal of Geophysical Research: Solid Earth, 125(2). https://doi.org/https://doi.org/10.1029/2019JB018390
47. Takebayashi, M., Onishi, M., & Iguchi, M. (2021). Large volcanic eruptions and their influence on air transport: The case of Japan. Journal of Air Transport Management, 97(December 2020), 102136. https://doi.org/10.1016/j.jairtraman.2021.102136
48. Webley, P., & Mastin, L. (2009). Improved prediction and tracking of volcanic ash clouds. Journal of Volcanology and Geothermal Research, 186(1–2), 1–9. https://doi.org/10.1016/j.jvolgeores.2008.10.022